Bilge International Journal of Science and Technology Research

Web : http://dergipark.gov.tr/bilgesci - **E-mail:** kutbilgescience@gmail.com

Received: 18.11.2019
Accepted: 23.12.2019
DOI: 10.30516/bilgesci.647923

ISSN: 2651-401X
e-ISSN: 2651-4028
3(Special Issue), 35-39, 2019

Controlling Structural and Electronic Properties of ZnO NPs: Density-Functional Tight-Binding Method

Mustafa Kurban[1*], Hasan Kurban[2], Mehmet Dalkılıç[2]

Abstract: We carried out a thorough examination of the structural and electronic features of undoped and Nitrogen (N)-doped ZnO nanoparticles (NPs) by the density-functional tight-binding (DFTB) method. By increasing the percent of N atoms in undoped ZnO NPs, the number of bonds (n), order parameter (R) and radial distribution function (RDF) of two-body interactions such as Zn-Zn, N-N, O-O, N-O, etc. were investigated using novel algorithms. Our results show that the total n of Zn-Zn interactions is greater than that of Zn-Zn, N-N, N-O, and O-O; thus, it means that Zn atoms have a greater preference for N or O atoms. The RDFs of Zn and O atoms increase based on the increase in the content of N atoms. The R of Zn, O and N atoms demonstrate that O and N atoms tend to locate at the center, whereas Zn atoms tend to reside on the surface. The density of state (DOS) indicates that the undoped and N-doped ZnO NPs demonstrate a semiconductor-like behavior that is coherent with measured data. The HOMO-LUMO energy gap decreases from -4.717 to -0.853 eV. n increase in the content of N atoms contributes to the destabilization of ZnO NPs due to a decrease in the energy gap.

Keywords: Productivity, Nanoparticle, N-doped ZnO, Electronic Structure, Data Science

1. Introduction

Nanoparticles (NPs), tiny objects whose sizes are lay between 1 and 100 nanometers, are finding use in diverse areas including energy, electronics, biomedical and optical fields due to their shape dependence properties as opposed to their bulk structure. More specifically, metallic NPs exhibit properties useful as both insulators and semiconductors and have been widely investigated (Wang, 2007; Yang, et al. 2008; Kushwaha, 2012). ZnO and its NPs, in particular, have been an area of intense scrutiny (Koç, et al. 2019; Rezkallah, et al. 2017; Caglar, et al. 2019; Coşkun, et al. 2018), because they have a wide bandgap and excellent optical properties for optoelectronics applications, being widely studied in various fields as photodetectors (Chang, et al. 2012), energetic materials (Barziniy, et al. 2019), and biomedical agents (Zhang, 2013).

This study aims at investigating the effect of Nitrogen (N) on ZnO NPs using the density-functional tight-binding (DFTB) method. Among the analyses, we conduct are studies of the HOMO, LUMO and HOMO-LUMO gap (E_g), total energies, density of states (DOS), as well as, the structural analysis such as radial distribution functions (RDFs), order parameter (R) to learn about how behave Zinc (Zn), Oxygen (O) and N atoms and the number of bonds (n) of two-body interactions in the undoped and doped ZnO NPs. To supplement our work on structural changes, we implemented programs in R code (https://github.com/hasankurban/Structural-Analysis-NanoParticles) to analyze the RDF, n and R.

2. Material and Method

We used the DFTB+ code (Aradi, et al. 2007), which is an implementation of DFTB method, with the 3ob/3ob-3-1 (Gaus, et al. 2013; Kubillus, et al. 2015) set of Slater Koster parameters to

[1]Kırşehir Ahi Evran University, Department of Electronics and Automation, 40100, Kırşehir, Turkey
[2]Indiana University, Bloomington, Computer Science Department, 47405, IN, USA.
*Corresponding author (İletişim yazarı): mkurbanphys@gmail.com

Citation (Atıf): Kurban, M., Kurban, H., Dalkılıç, M., (2019). Controlling Structural and Electronic Properties of ZnO NPs: Density-Functional Tight-Binding Method. Bilge International Journal of Science and Technology Research, 3(Special Issue): 35-39.

compare the structural features and electronic structure of studied ZnO NPs.

To make the program more accessible to non-computational scientists, we have also ensured that the programs are simple to use. Additionally, we have added functionality to include analysis of the *n*, *R*, and RDF of the ZnO NPs in terms of an increase in the N content. The code is open source and it is freely available online, thus, researchers can visualize their data using the code.

3. Results

3.1. Structural analysis

The initial structure of undoped ZnO NP with n = 258 atoms is indicated in Fig. 1. All of the ZnO NPs were characterized by 30×30×30 supercells of the hexagonal crystal structure (wurtzite, space group *P6₃mc*). We *carved* a spherical ZnO NP from this bulk hexagonal *supercell*. The radius of the NP is set to the desired value (0.9 nm) and only atoms within that sphere are considered, whereas those outside the sphere are removed. All calculations are carried out at constant volume.

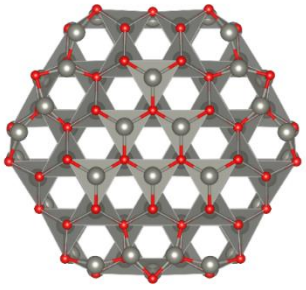

Figure 1. Initial structure (polyhedral) of undoped ZnO NP with 258 atoms. (Red is Oxygen, grey is Zinc).

The n_{ij} represents the nearest neighbor contacts number, which is also the number of bonds, and usually used to distinguish the degree of packing, a significant property of NP. The n_{ij} (Wu, et al. 2016) for the NPs is given by

$$n_{ij} = \sum_{i<j} \delta_{ij} \qquad (1)$$

where $\delta_{ij} = \begin{cases} 1, r_{ij} \leq 1.2 r_{ij}^{(0)} \\ 0, r_{ij} > 1.2 r_{ij}^{(0)} \end{cases}$ $i, j =$ Zn, O or N, r_{ij} is the distance between i and j atoms and $r_{ij}^{(0)}$ is obtained by fitting the experimental data and represents a nearest neighbor criterion (NIST, 2019; Czajkowski, et al. 1999). Fig. 2 indicates the total n in the ZnO NP with 258 atoms. The curve of ZnO NP in Fig. 2 reveals that the n of N-N and N-O interactions increases gradually in terms of increase in the content of N. Moreover, the total n of Zn-Zn interactions is comparatively smaller than the total n, while the n of N-N is the smallest. These results show that N atoms incline to make more bonds with O atoms: that Zn_2 tends to locate at the surface. Additionally, the total n of Zn-Zn bonds is larger than that of N-N, N-O, O-O and Zn-Zn. it means that Zn atoms have a higher priority for N or O atoms than for Zn atoms based on the increase of N content. Here, it is interesting to note that there is no experimental data on the Zn-O and Zn-N two-body interactions, thus, Zn atoms probably adhere to N or O atoms.

R_{T_i} represents the order parameter and is used to find a stable structure in the NP. One needs to calculate R_{T_i} (Kurban, et al. 2016) which helps to investigate the segregation of atoms in the NP. R_{T_i} is the average distance of a type T_i atoms according to a center of a NP,

$$R_{T_i} = \frac{1}{n_{T_i}} \sum_{i=1}^{n_{T_i}} r_i \qquad (2)$$

where is the number of T_i type atoms, and r_i is the distance of the atoms to the coordinate center . We define a distance from the center of NP to a reference point as ϵ to indicate the location of atoms; if $R_{T_i} < \epsilon_{min}$ (a "small" value), the T_i type atoms are assumed to be at the center, and if $R_{T_i} > \epsilon_{max}$ (a "large" value), the T_i type atoms are assumed to be at the surface region of NP. If neither is true, *i.e.*, if $\epsilon_{min} \leq R_{T_i} \leq \epsilon_{max}$ (a "medium" value), it is assumed a well-mixed NP.

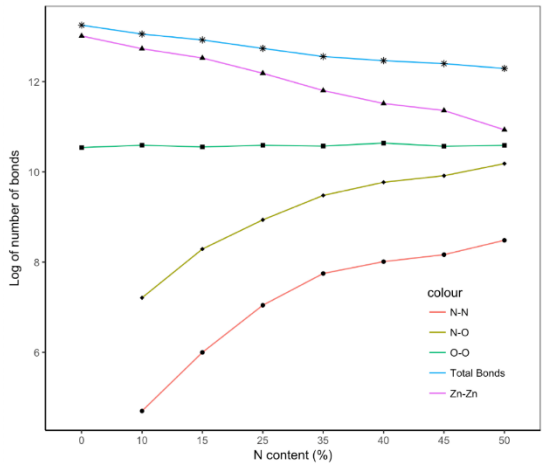

Figure 2. The number of bonds of binary N-N, N-O, O-O and Zn-Zn interactions based on an increase in the content of N atoms.

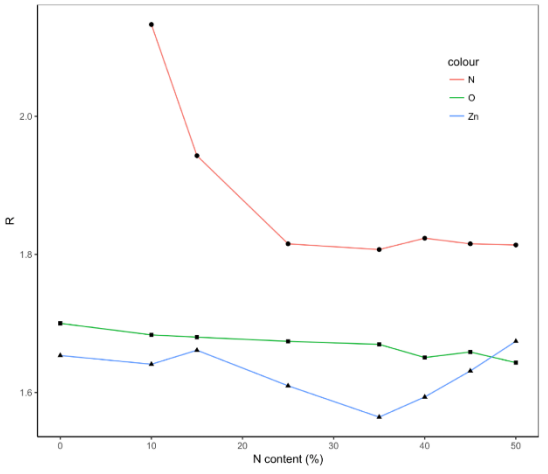

Figure 3. The order parameter of Zn, O and N atoms in the ZnO NPs.

Fig. 3 demonstrates the *R* of Zn, O and N atoms based on the N content in the ZnO NPs. Here, the *R* shows the changes in the structural properties of ZnO NP with a change N-doped ZnO NPs. The *R* of Zn, O and N atoms indicate that N atoms incline to locate at the center, while Zn atoms tend to occupy the surface. The *R* of N atoms to the surface is related to its lower cohesive energy. Besides, the *R* demonstrates different features when it comes to an increase in the content of N atoms. For example, R_{Zn} values sharply increase after doping 35% N, and R_O smoothly decrease.

The Radial Distribution Function (RDF), a significant parameter, is known as the probability of finding a particle at a distance *r* from another tagged particle. The RDF is mathematically shown as follows:

$g_{(r_i)} = n_{(r_i)}/(|\Delta| \times V_s \times V_d)$ where $n_{(r_i)}$ represents the mean number of atoms in a shell of width dr at distance r_i, $|\Delta|$ is the total atom number and V_s is the volume of the spherical shell and V_d is the mean atom density.

Fig. 4 indicates the RDF Zn-Zn, O-O and N-N two-body interactions in the studied ZnO NPs. The RDFs are searched for each interactions of optimized NPs. Zn-Zn has a narrower and higher distribution than O-O interactions. With regards to an increase in the content of N, the peaks for both pairs increase. Moreover, the fluctuations were observed in obvious peaks of N-N interactions with raising the content of N.

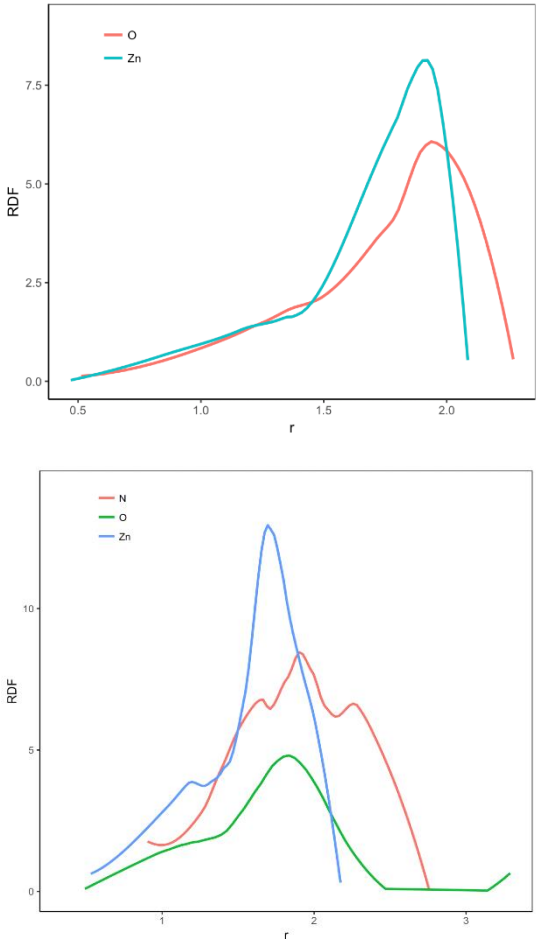

Figure 4. Radial distribution function of undoped (up) and doped (down) ZnO NPs.

3.2. Electronic structure

In Fig. 5, we demonstrate the results of the HOMO, LUMO and Fermi levels with respect to N content to acquire detailed information on electronic states in the undoped and N-doped ZnO NPs. When it comes to an increase in the content of N, the density of localized states concomitantly decreases, thus the greatest contribution comes from the undoped ZnO NPs and then these fluctuations progressively also disappear. It has a sharply increasing tendency to occur in the region of between -10 and -15 eV. The DOS figures also demonstrate that the studied ZnO NPs have the energy gap, so, all the NPs indicate semiconductor character. With increasing the content of N, the changes in HOMO, LUMO and Fermi energy were predicted in a different manner like an increase and a decrease.

The HOMO energy level for undoped ZnO NP is -7.89 eV, *i.e.*, about 0.97 eV higher than that of the 50% N-doped NP (-6.91 eV) which is the lowest HOMO level among the other NPs models and thus it is less reactive, but more stable (see Fig. 6, Table 1). On the other hand, Fermi energies are in the middle of the valence and conduction band. The HOMO-LUMO energy gap of undoped ZnO NP is 4.71 eV, which decreases from -4.717 to -0.853 eV. It is clear then that an increase in the content of N atoms contributes to the destabilization of ZnO NPs due to a decrease in the energy gap.

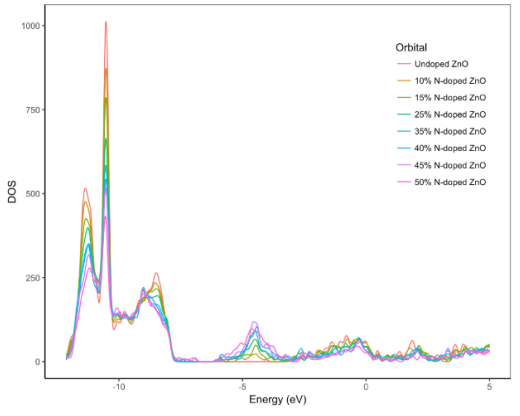

Figure 5. The total density of states (DOS) of undoped and N-doped ZnO NPs.

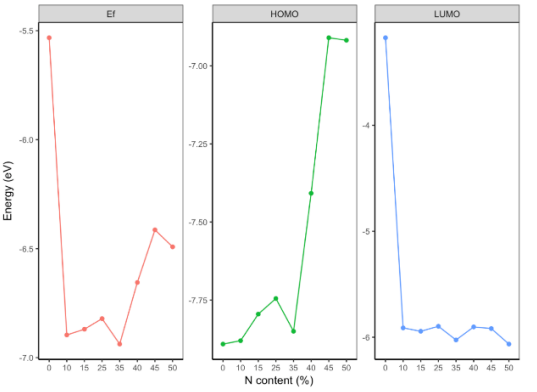

Figure 6. HOMO, LUMO and Fermi energies of undoped and N-doped ZnO NPs.

Table 1. The electronic properties such as HOMO (H), LUMO (L), Energy gap (E_g), and Fermi energy (E_F) of undoped and N-doped ZnO NPs.

	H	L	E_g	E_F
Undoped ZnO	-7.89	-3.17	4.71	-5.53
10% N-doped	-7.88	-5.91	1.96	-6.89
15% N-doped	-7.79	-5.94	1.85	-6.86
25% N-doped	-7.74	-5.89	1.84	-6.82
35% N-doped	-7.85	-6.02	1.82	-6.93
40% N-doped	-7.40	-5.90	1.50	-6.65
45% N-doped	-6.91	-5.91	0.99	-6.41
50% N-doped	-6.91	-6.06	0.85	-6.49

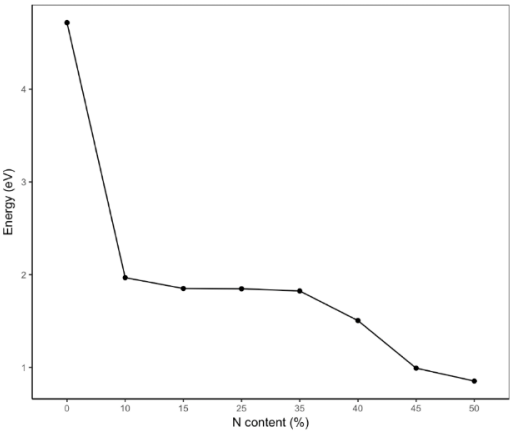

Figure 7. HOMO-LUMO energy gap of undoped and N-doped ZnO NPs.

4. Discussion and Conclusions

In this study, we use the DFTB method and study electronic structural features of undoped and Nitrogen (N)- doped ZnO NPs with 258 atoms. To carry out structural analysis, we developed a

new code in R code to conduct structural analysis, i.e., analyzing the RDF, *n* and *R* of two-body interactions of atoms in the ZnO NPs. Our results show that the total *n* of Zn-Zn two-body interactions is larger than that of N-N, N-O, O-O, and Zn-Zn; thus, it means that Zn atoms have a higher priority for N or O atoms. N atoms contribute to the stabilization of the ZnO NPs. The *R* of Zn, O and N atoms indicate that N atoms tend to locate at the center, while Zn atoms incline to occupy the surface. The HOMO decreases; however, the LUMO increase, thus the HOMO-LUMO band gap declines from 4.717 to 0.853 eV. The decline in the HOMO value contributes to the stabilization of the ZnO NPs. The DOS analysis also shows that ZnO NPs exhibits a semiconductor-like character.

Acknowledgements

The calculations were partially carried out at TUBITAK ULAKBIM, High Performance and Grid Computing Centre (TRUBA resources), Turkey.

Kaynaklar

Aradi, B., Hourahine, B., Frauenheim, T. (2007). DFTB+, a Sparse Matrix-Based Implementation of the DFTB Method. J. Phys. Chem. A 111, 5678-5684.

Barzinjy, A. A., Mustafa, S., Ismael, H. H. J. (2019). Characterization of ZnO NPs Prepared from Green Synthesis Using Euphorbia Petiolata Leaves. EAJSE 4, 74-83.

Caglar, M., Ilican, S., Caglar, Y., Yakuphanoglu F. (2019). Electrical conductivity and optical properties of ZnO nanostructured thin film. Appl. Surf. Sci. 255, 4491-4496.

Chang S-P., Chen, K-J. (2012). Zinc Oxide NP Photodetector. J. Nanomater. 2012, 1-5.

Coşkun, B., Mensah-Darkwa, K., Soylu, M., Al-Sehemi, A. G., Dere, A., Al-Ghamdi, A., Gupta, R.K., Yakuphanoglu, F. (2018). Optoelectrical properties of Al/p-Si/Fe:N doped ZnO/Al diodes. Thin Solid Films 653, 236-248.

Czajkowski, M. A., Koperski, J. (1999). The Cd2 and Zn2 van der Waals dimers revisited. Correction for some molecular potential parameters. Spectrochim. Acta, Part A 55, 2221-2229.

Gaus, M., Goez, A., & Elstneri, M. (2013). Parametrization and Benchmark of DFTB3 for Organic Molecules. J. Chem. Theory Comput. 9, 338-354.

Koç, M. M., Aslan, N., Erkovan, M., Aksakal, B., Uzun, O., Farooq, W. A., Yakuphanoğlu, F. (2019). Electrical characterization of solar sensitive zinc oxide doped-amorphous carbon photodiode. Optik 178, 316-326.

Kubillus, M., Kubař, T., Gaus, M., Řezáč, J., & Elstner, M. (2015). Parameterization of the DFTB3 Method for Br, Ca, Cl, F, I, K, and Na in Organic and Biological Systems. J. Chem. Theory Comput. 11, 332–342.

Kurban, M. (2018). Size and composition dependent structure of ternary Cd-Te-Se nanoparticles. Turk. J. Phys. 42, 443-454.

Kurban, M. Malcıoğlu, O. B. Erkoç Ş. (2016). Structural and thermal properties of Cd-Zn-Te ternary NPs: Molecular-dynamics simulations. Chem. Phys. 464, 40-45.

Kushwaha, A. K. (2012). Lattice dynamical calculations for HgTe, CdTe and their ternary alloy CdxHg1−xTe. Comp. Mater Sci. 65, 315-319.

NIST Standard Reference Database (2019). Experimental bond lengths. https://cccbdb.nist.gov/expbondlengths1.asp. (Access Date: 10.05.2019).

Rezkallah, T., Djabri, I., Koç, M. M., Erkovan, M., Chumakov, Yu., Chemam, F. (2017). Investigation of the electronic and magnetic properties of Mn doped ZnO using the FP-LAPW method. Chin. J. Phys. 55, 1432-1440.

Wang, CL., Zhang, H., Zhang, JH., Li, MJ., Sun, HZ., Yang, B. (2007). Application of Ultrasonic Irradiation in Aqueous Synthesis of Highly Fluorescent CdTe/CdSCore-Shell Nanocrystals. J. Phys. Chem. C111, 2465-2469.

Wu, X., Wei, Z., Liu, Q., Pang, T., Wu, G. (2016). Structure and bonding in quaternary Ag-Au-Pd-Pt clusters. J Alloy. Compd. 687, 115-120.

Yang, P., Tretiak, S., Masunov, A. E., Ivanov, S. (2008). Quantum chemistry of the minimal CdSe clusters. J. Chem. Phys. 129, 074709-1—074709-12.

Zhang, Y., Nayak, TR., Hong, H., Cai, W. (2013). Biomedical applications of zinc oxide nanomaterials. Curr. Mol. Med. 13(10), 1633-1645.